AD-A031 555

Electronic Design of a Slant-Range Optical Proximity Sensor

September 1976

U.S. Army Materiel Development
and Readiness Command
HARRY DIAMOND LABORATORIES
Adelphi, Maryland 20783

TM-76-16—Electronic Design of a Slant-Range Optical Proximity Sensor—by Jonathan Vanderwall

The findings in this report are not to be construed as an official Department of the Army position unless so designated by other authorized documents.

Citation of manufacturers' or trade names does not constitute an official indorsement or approval of the use thereof.

Destroy this report when it is no longer needed. Do not return it to the originator.

UNCLASSIFIED

SECURITY CLASSIFICATION OF THIS PAGE *(When Data Entered)*

REPORT DOCUMENTATION PAGE		READ INSTRUCTIONS BEFORE COMPLETING FORM
1. REPORT NUMBER HDL-TM-76-16	2. GOVT ACCESSION NO.	3. RECIPIENT'S CATALOG NUMBER
4. TITLE *(and Subtitle)* Electronic Design of a Slant-Range Optical Proximity Sensor		5. TYPE OF REPORT & PERIOD COVERED Technical Memorandum 6. PERFORMING ORG. REPORT NUMBER
7. AUTHOR(s) Jonathan Vanderwall		8. CONTRACT OR GRANT NUMBER(s) DA: 1W362616AH77
9. PERFORMING ORGANIZATION NAME AND ADDRESS Harry Diamond Laboratories 2800 Powder Mill Road Adelphi, MD 20783		10. PROGRAM ELEMENT, PROJECT, TASK AREA & WORK UNIT NUMBERS Program: 6.26.16.A
11. CONTROLLING OFFICE NAME AND ADDRESS US Army Materiel Development & Readiness Command Alexandria, VA 22333		12. REPORT DATE September 1976 13. NUMBER OF PAGES 33
14. MONITORING AGENCY NAME & ADDRESS*(if different from Controlling Office)*		15. SECURITY CLASS. *(of this report)* Unclassified 15a. DECLASSIFICATION/DOWNGRADING SCHEDULE

16. DISTRIBUTION STATEMENT *(of this Report)*

Approved for public release; distribution unlimited.

17. DISTRIBUTION STATEMENT *(of the abstract entered in Block 20, if different from Report)*

18. SUPPLEMENTARY NOTES

HDL Project: A77593
DRCMS Code: 662616.11.H7700

19. KEY WORDS *(Continue on reverse side if necessary and identify by block number)*

Optical fuze
Laser transmitter
Laser receiver
Electro-optical sensor
Injection laser modulator

20. ABSTRACT *(Continue on reverse side if necessary and identify by block number)*

This paper describes the electronic design of a slant-range optical proximity sensor using a pulse-modulated injection laser for the transmitter and a direct-detection receiver for the collection of target returns, much after the manner of a conventional pulse-radar. Of particular interest is the development of laser modulator circuitry to produce 50-A pulses up to 200 ns wide at repetition rates up to 2 kHz.

DD FORM 1 JAN 73 1473 EDITION OF 1 NOV 65 IS OBSOLETE

UNCLASSIFIED

SECURITY CLASSIFICATION OF THIS PAGE *(When Data Entered)*

CONTENTS

APPENDICES

FIGURES

1. INTRODUCTION

In a companion paper,[1] Sztankay has defined the system properties required to achieve an acceptable level of performance in an optical slant-range proximity sensor. The present paper describes the design of electronic circuitry developed to evaluate the feasibility of these concepts, while a third paper, by Holland and Wellman,[2] brings the study to its fruition by recounting the results obtained experimentally. This is not to say that the circuitry discussed here is suitable only for evaluation. On the contrary, a guiding principle throughout was to develop circuits that could readily be adapted to production and that would operate reliably with a minimum of dependence on device parameters. Basically, the system involves the generation of an impulse of infrared radiation (λ = 905 nm) of several tens of watts peak amplitude by means of a GaAs injection laser, the optical focussing of the radiation in the direction of the supposed target, the collection of returns from the target, and their detection, amplification, and display. Unlike a typical radio proximity sensor operating on a homodyne principle, the transmitter and receiver are in this case independent of one another and are therefore described separately. Let us begin by discussing the transmitter.

At the outset of this work, several types of GaAs lasers were considered suitable for investigation: The RCA types SG2007 (single diode), TA7765 (stack of two diodes), and SG3001 (stack of three diodes). It is interesting to tabulate a few of their properties:

Type	P_o (W)	I_{fm} (A)	Source size (mils)
SG2007	25 min	75	24 × 0.08
TA7765	50 min	100	25 × 4
SG3001	25 min	40	10 × 10

(Similar diodes are available from other sources.)

---

[1] *Z. G. Sztankay, Analysis of a Slant-Range Optical Proximity Sensor (U), Harry Diamond Laboratories TR-1625 (July 1973).*

[2] *R. Holland and R. Wellman, Feasibility Demonstration of a Slant Range Optical Proximity Sensor (U), Harry Diamond Laboratories TM-74-17 (December 1974).*

It is at once apparent that the SG3001 stack of three diodes is superior in watts per ampere. Furthermore, the emissive area of the SG3001 is within a 10-mil square, whereas the other units have maximum dimensions of 24 and 25 mils. Thus, for a lens of given focal length, the maximum divergence of the transmitted beam by using a stack of three diodes is less than half that of the single diode or stack of two diodes. This type therefore formed the basis of most of the experimental transmitters used in this study.

Sztankay[1] develops the relations whereby the transmitter output pulse is defined in terms of system parameters. From these definitions and the characteristics of the injection laser, he develops also the properties required of the pulsed injection current, i.e., the pulse repetition frequency (f_r), the pulse width (t_w), the required peak current (I_{pk}), and the pulse rise and fall times (t_r and t_f). Briefly, the optical pulse is definable from the same considerations that prevail in the design of a conventional pulsed radar (e.g., detection probability determines peak power required). From this, it emerged as desirable to attain the greatest possible power output and hence to design for the largest permissible injection current, I_{fm}, namely, 40 A for the SG3001 stack. The pulse width was not considered to be a fixed parameter, but rather an experimental variable ranging from 50 to 200 ns.

2. BASIC TRANSMITTER CIRCUIT

The only type of solid-state device then able to switch large current for periods up to 200 ns was a fast, high-current silicon-controlled rectifier (SCR), and the simplest application of it was as a switch to connect the laser diode or stack to a previously charged energy storage capacitor (fig. 1). This circuit requires the addition of several parts if it is to operate properly (fig. 2). Diode D1 prevents the very large discharge pulse developed across the laser diode stack (LDS) from harming Q1 (by reverse breakdown of the gate-cathode junction) and, by the same token, prevents the discharge pulse from finding its way into the gate pulse generator. Resistor R1 prevents the gate of Q1 from "floating up" through leakage to the point at which false triggering is likely. Moreover, it increases the maximum dV/dt that may be developed across the untriggered SCR without risking rate-effect triggering. We recur to this important consideration later in this report.

---

[1] *Z. G. Sztankay, Analysis of a Slant-Range Optical Proximity Sensor (U), Harry Diamond Laboratories TR-1625 (July 1973). (CONFIDENTIAL)*

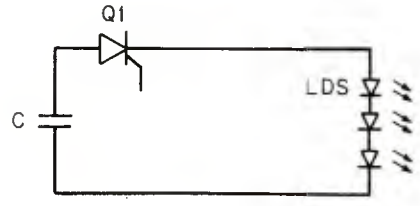

Figure 1. Basic transmitter circuit.

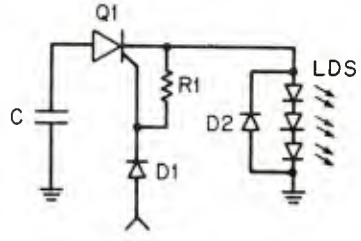

Figure 2. Practical transmitter circuit.

The discharge path C-Q1-LDS contains also a certain amount of stray series inductance. The equivalent circuit during discharge is therefore a series RLC circuit, with R comprising the instantaneous resistances of the laser and the SCR strongly nonlinear. If the circuit is underdamped, the current through LDS ultimately reverses. The manufacturer states in strong terms that reverse current should be prevented, with a chance of catastrophic failure if it is not, and recommends the use of one or more clamp diodes in shunt with the laser. This clamp diode appears as D2 in figure 2. The amplitude and shape of the current pulse can be determined by a current probe placed over the laser diode anode lead. Commercially available probes that have proved satisfactory for this purpose are the Tektronix CT-2 and the American Laser Systems model 711.

For pulse widths of 50 to 200 ns, the parasitic inductance and the storage capacitor are the principal elements in determining the rise time, fall time, and width of the current pulse. For a given design, it is plainly best to determine the relationship empirically. As a rough guide, however, appendix A shows graphs relating the measured current pulse parameters to various values of storage capacitance and applied voltage. For lasers such as these in which the lasing threshold current I_{th} is on the order of 0.3 I_{fm} (e.g., I_{th} = 12 A, I_{fm} = 40 A), the optical pulse inevitably is shorter than the current pulse

that generates it and, moreover, has shorter rise and fall times. Because of the variability of series inductance from one design layout to another and the variability of I_{th} from one laser diode to another, it was not considered worthwhile to attempt analytic prediction of the optical pulse parameters. Again, by resorting to measurement, one arrives at a rough approximation: In the example given, the optical pulse rise and fall times are about 0.7 of the current pulse rise and fall times for $I_{pk} > 2\ I_{th}$. The optical pulse width at $I_{pk} = I_{fm}$ is on the order of 0.85 to 0.9 of the current pulse width.

3. CHARGING CIRCUITS

3.1 Resistor Charging

Numerous practical schemes exist for replenishing the energy store after each discharge. The scheme that a designer may elect to use depends on the application and the devices available. For example, the easiest means of recharging C in figure 2 is to add a resistor and voltage source V_s (fig. 3). It is often the case that the capacitor must be charged nearly to forward breakover voltage V_{fx} of the SCR. To charge C to, say, 0.95 V_s requires $t = 3$ RC s. When the SCR is triggered, the voltage V_c drops to some value that is small compared to V_s, and a current $I \simeq V_s/R$ flows through the resistor and SCR. If $V_s/R > I_h$, the SCR holding current, then the SCR latches in the conducting state. This latching establishes a minimum value for R and hence a limitation of f_r. The SCR used for the greater part of the present work has I_h(min) of 0.3 mA at 25°C: If $V_s = 100$ V, R > 333 kilohms prevents latching. Suppose, however, that the intended application requires $f_r = 1$ kHz and that considerations of energy and pulse width have already established C = 0.02 μF. Then 3 RC = 0.018 s, so that the maximum repetition frequency becomes 56 Hz.

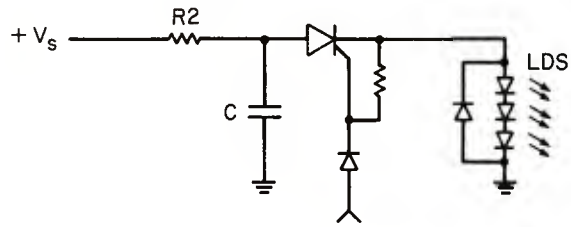

Figure 3. Resistor charging.

An interesting means of circumventing this limitation is suggested by DeVilbiss and Klunk[3] (fig. 4). In this circuit, the principal source of charging current is the transistor Q1, normally biased on by way of resistor R1 and thus charging C_a by way of R2. When the SCR is triggered into conduction, diodes D_a and D_b are forward biased, thus placing a reverse bias on Q1 and turning that unit off. Thus, the only remaining current available is supplied by R1, which may be made sufficiently high to prevent the SCR from latching in its conducting state. Although this method allows a high PRF to be attained, it was not considered for development in this project for several reasons.

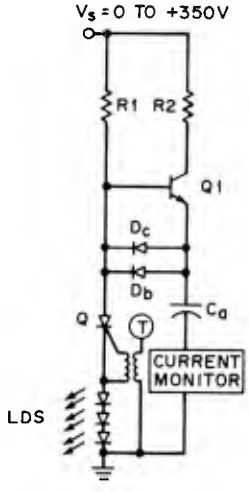

Q = 40768, T = 1:1 PULSE TRANSFORMER SPRAGUE 11Z12
D_a, D_b = IN914
C_a = 0.022μF, 400V FOR ARRAYS OF UP TO 20 DIODES IN SERIES
R1 = 35k, 1/2W
R2 = 39k, 2W
Q1 = 2N3439 WITH HEAT SINK

Figure 4. Transistor-aided charging (from W. F. DeVilbiss and S. L. Klunk, RCA Application Note AN-4469 (February 1971).

[3] *W. F. DeVilbiss and S. L. Klunk, Solid-State Pulse Power Supplies for RCA GaAs Injection Lasers, RCA Application Note AN-4469 (February 1971).*

First, no resistive charging circuit can be more than 50 percent efficient. Second, the diodes D_a and D_b must carry the entire discharge current, and it did not appear advisable at that time to depend on diodes of the 1N914 type to carry currents of ~20 to ~50 A. Furthermore, the diodes introduce additional series resistance and inductance in the high-current path, and it was the intention to minimize these quantities wherever possible. Lastly, the initial experiments employed an SCR that required 600 V on C = 0.04 μF to develop 80 A in the laser. It was not considered feasible to try to develop for low-cost production a design requiring a transistor having $BV_{ceo} > 600$ V. Consequently, some other means of recharging the capacitor were sought, with several objectives in view. First, the circuit would have to work over a large range of V_s to secure a wide range of I_{pf} for research. Second, it should have provision for varying PRF up to a maximum of at least 2 kHz. Third, it was hoped to make the circuit operation insensitive to certain parameters of the SCR, notably holding current I_h and recovery time t_{fbr}. Fourth, as a basic design point, a charging method that theoretically was lossless was considered preferable to some method that was not.

3.2 Resonant Charging

Such a theoretically lossless method is depicted in figure 5, in which the charging resistor of figure 3 has been replaced by a diode and inductor (D3 and L1). The operation of this arrangement is readily described. Assume that C1 has been entirely discharged and that the SCR has reverted to its nonconducting state at t = 0. Diode D3 is forward biased, and C1 begins to charge via L1. Assuming ideal components, the current that flows is a half sinusoid:

$$i = i(t) = V_s \left(\frac{C1}{L1}\right)^{\frac{1}{2}} \sin \frac{t}{(L1C1)^{\frac{1}{2}}}, \text{ for } 0 < t < \pi(L1C1)^{\frac{1}{2}} . \quad (1)$$

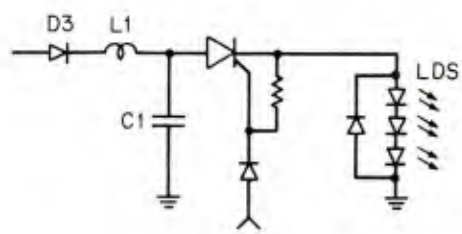

Figure 5. Resonant charging.

For $t > \pi(L1C1)^{\frac{1}{2}}$, the current in D3-L1-C1 reverses, shutting off D3 and ending the charging process. Over the same interval, the voltage on C1 rises according to

$$V_c = V_s \left[1 - \cos \frac{t}{(L1C1)^{\frac{1}{2}}}\right], \qquad (2)$$

so that at the end of the charging interval, $V_c = 2\ V_s$. Importantly, this last result does not depend on the values of L1 and C1, as these merely establish the length of the charging interval. (The effect of nonideal components is considered at length in appendix B. Briefly, the charging time is virtually unaffected, but the voltage to which the capacitor charges may be significantly less than $2\ V_s$.)

This circuit has a serious practical drawback: the charging current may not be allowed to rise so fast that the holding current of the SCR is exceeded before it can recover to its blocking state. This drawback requires a very large inductance and, moreover, violates the design goal of desensitizing the circuit to variations in I_h and t_{fbr}. Conceptually, the most direct method of eliminating this dependence on device parameters is to arrange that V_s be connected to begin the charging interval at $t = 0$ and disconnected at some time $t_1 > \pi(L1C1)^{\frac{1}{2}}$, before triggering the SCR. Since no source of holding current exists, specification of I_h becomes irrelevant. Similarly, by delaying the reconnection of V_s, the recovery time may be rendered inconsequential.

3.3 Resonant Charging from a Switched-Supply Charging Circuit

The development of a switched-supply charging circuit would appear at first to present the same difficulty as did the circuit of figure 4. Namely, a relatively high-voltage switching element is required, even though the voltage doubling property of the resonant charging circuit alleviates this problem to a degree. Referring to the operation of the circuit of figure 5, at the end of the charging interval, D3 is cut off by the reversal of current flowing in L1-C1. One might replace D3 by an SCR that could be fired to connect V_s and that would automatically disconnect V_s in the same manner as the diode. This replacement has a twofold advantage over transistor switching. First, the cost of an SCR that can block several hundred volts is trivial, because such components are used widely in consumer products. Second, the driving circuitry is much simplified, since the SCR requires only a trigger, whereas the transistor must be held in saturation throughout the desired interval. This substitution is made in figure 6 (compare with fig. 5), in which Q2 takes the place of D3.

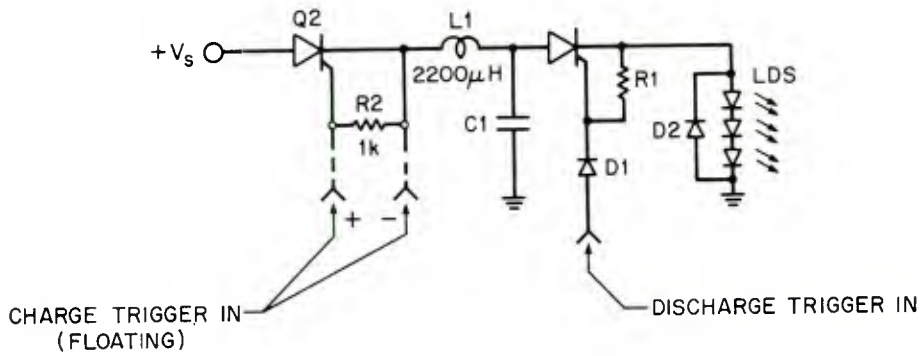

Figure 6. Basic SCR-switched resonant charging.

The rate of rise of V_c, the voltage on C1, may not exceed $dV/dt|_{crit}$, the critical rate of rise of the anode voltage of Q2. From equation (2), one may easily determine the maximum dV_c/dt, obtaining

$$\max \frac{dV_c}{dt} = V_s (L1C1)^{-\frac{1}{2}} \quad , \tag{3}$$

which, to prevent Q2 from being rate-effect triggered, must satisfy the inequality

$$\frac{dV}{dt}\Big|_{crit} > V_s \, (L1C1)^{-\frac{1}{2}} \quad . \tag{4}$$

Solving for L1,

$$L1 > \frac{1}{C1} \left(\frac{V_s}{\frac{dV}{dt}\Big|_{crit}} \right)^2 \quad . \tag{5}$$

From equations (5) and (2), the time to recharge C1 must satisfy

$$t > \frac{V_s}{\frac{dV}{dt}\Big|_{crit}} \quad . \tag{6}$$

In the case at hand, V_s = 50 V, and $dV/dt|_{crit}$ = 20 V/μs. Substitution of these values in equation (6) yields

$$t > 7.85\ \mu s\ . \qquad (7)$$

Further, if C1 = 0.022 μF, the minimum value for L1 may be obtained. From equation (5), L1 > 310 μH prevents rate-effect triggering.

This is a reasonable value. L1 is realizable in a small package, and the time to recharge is short. The implementation of the circuit of figure 6 was not, however, trouble free. It was discovered that, with the capacitor charged, firing Q1 resulted in the rate-effect retriggering of Q2. Thus, Q1 and Q2 conduct simultaneously, disabling the circuit and often destroying one or more components.

A brute-force solution was contrived (fig. 7). Four components have been added: R3, R4, D4, and D5. Their operation is readily described, beginning with C1 discharged and a charge trigger applied to the gate of Q2. With Q2 fired, C1 charges to 2 V_S through Q2, D4, and L1. At the end of the charging interval defined by the values of L1 and C1, the current reverses, shutting off D4. Resistor R3 is made large enough so that it alone cannot hold Q2 in conduction. Q2 therefore turns off, and the voltage at point x decreases to 0 V as R3 discharges whatever stray capacitance may be present. Then it is possible to apply a trigger to Q1, initiating the discharge of C1; the negative spike coupled back to point x via the self-capacitance of L1 and the depletion capacitance of D4 is promptly dissipated in R4-D5, and thus rate effect cannot trigger Q2.

The entire circuit as used for experiment is given in figure 8. With the components shown, the charging circuit accepts V_S from about 30 to 300 V, thus permitting study of widely disparate SCR types in the discharge circuit. This purpose is served also by constructing the circuit in two pieces, one comprising essentially the laser in its discharge circuit and the other comprising the timing, triggering, and charge-enable circuits. Unijunction transistor Q1, operating as a relaxation oscillator, generates a train of pulses at a rate selected by switch S2. The timing resistors were chosen to give repetition rates of approximately 100, 200, 500, and 1000 Hz. The sawtooth waveform appearing at the emitter of Q1 is differentiated by C6, and the resulting negative-going spike triggers Q2, a programmable UJT operating as a one-shot. The pulse thus generated at the cathode of Q2 is coupled via T1 to the charging SCR Q8 to initiate the charging of the energy storage capacitor and via C8 to an emitter-coupled delay one-shot comprising transistors Q3, Q4, and Q5. The period of the one-shot is about 260 μs, long enough for the charging process to be completed and the stray capacitances to be discharged as described above.

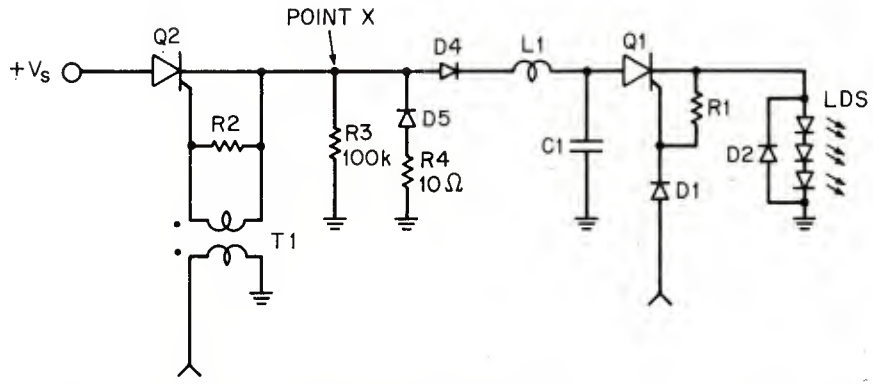

Figure 7. Practical SCR-switched resonant charging.

At the end of the delay time, a negative-going step appears at the collector of Q4. The step is differentiated by C10 to trigger Q6, another programmable UJT in a one-shot circuit identical to that of Q2. The pulse generated at the cathode of Q6 is led off via cable K2 to trigger the discharge SCR, located remotely at the laser head. As a measurement convenience, a scope trigger pickoff circuit was included; this comprises resistors R14 to R17 and switch S3, allowing the operator to select a scope trigger from either of the programmable UJT one-shots.

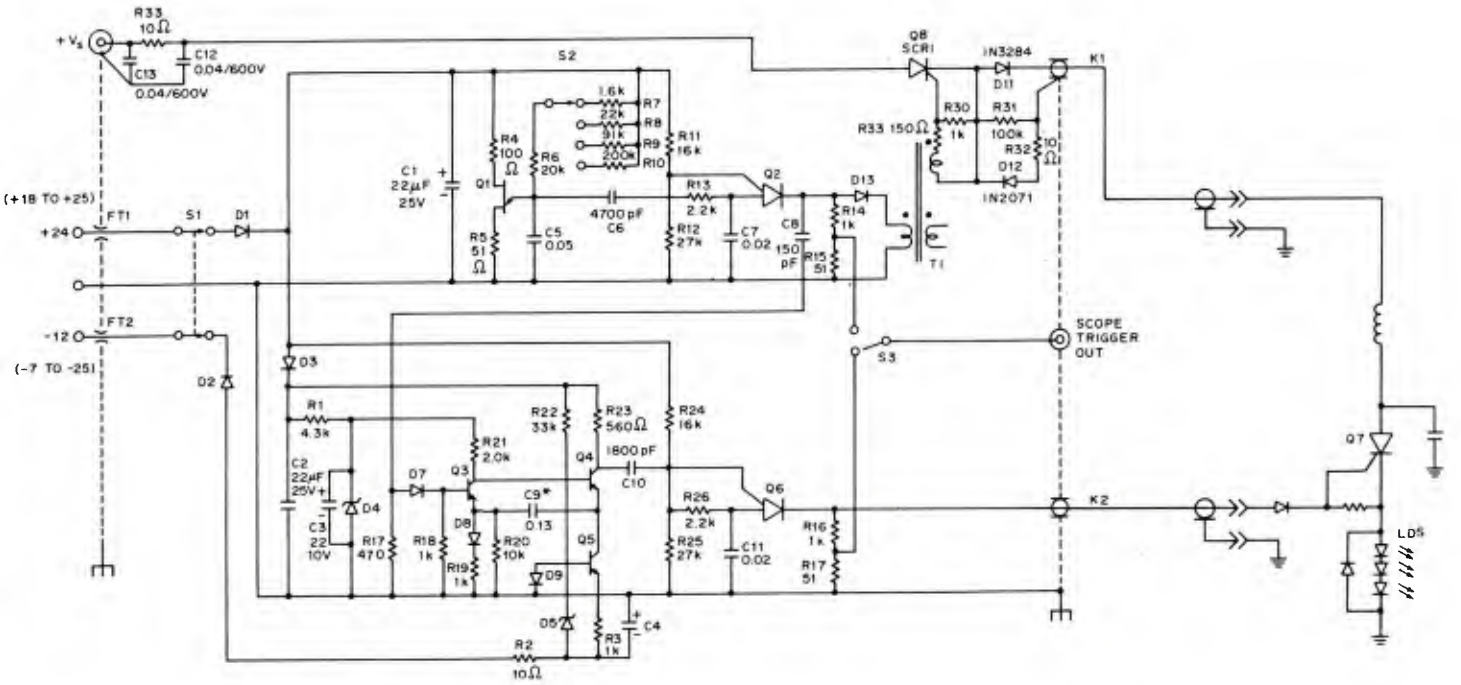

Q1--2N2646
Q2,Q6--D13T1
Q3,Q4--2N2222
Q5--2N2102

SCR1--MCR1336-10
T1--PULSE ENGINEERING TYPE PE2229, 1:1:1
D1,D2--1N2069

D3,D6,D10--1N914
D4--1N759A--10-V ZENER
D5--5.0-V ZENER
D7,D8,D9--HPA TYPE 5082-2230

Figure 8. Entire transmitter circuit.

3.4 Remarks

The field performance of the laser pulsers is covered by Holland and Wellman[2] and is thus not included here. However, it is useful to sum up the thrust of the development of pulser circuits. The advent of SCR's which give very rapid rise times and low loss at currents of 40 to 50 A has made it comparatively easy to design reliable circuits to drive injection lasers to their full outputs. Only in devising circuits to recharge the storage capacitors do problems arise. For those applications in which a repetition rate of a few tens of hertz suffices, a simple resistive charging scheme is possible. Beyond this rate, the properties of the SCR require, first, that the charging current be interrupted before the discharge may be triggered; second, that adequate recovery time be allowed before the charging current resumes; and third, that the critical rate of rise of the anode voltage not be exceeded during the charging interval. The means developed for these requirements give the designer good control over these quantities and at the same time are theoretically lossless, useful when the available input power may be limited.

4. RECEIVER

The receiver used in this evaluation was of extremely simple design (fig. 9). The characteristics of the optical system are covered in the concurrent papers.[1,2] Briefly, lens L gathers incident light flux and focusses it upon the active area of the avalanche photodiode (APD). Band-pass filter F acts as an optical preselector, thus improving S/N by rejecting a considerable part of the background radiation. The flux incident upon the APD gives rise to a photocurrent, which is multiplied by the avalanche multiplication factor M. The multiplied photocurrent is coupled to a transimpedance amplifier, which develops an output voltage proportional to input current. A further stage of voltage amplification is provided to raise the signal to a level convenient for driving an oscilloscope. Gain control is effected by manually varying the bias voltage to the APD, a range of 20 to 40 dB being available, depending on the type of diode used.

---

[1] *Z. G. Sztankay, Analysis of a Slant-Range Optical Proximity Sensor (U), Harry Diamond Laboratories TR-1625 (July 1973). (CONFIDENTIAL)*

[2] *R. Holland and R. Wellman, Feasibility Demonstration of a Slant-Range Optical Proximity Sensor (U), Harry Diamond Laboratories TM-74-17 (December 1974). (CONFIDENTIAL)*

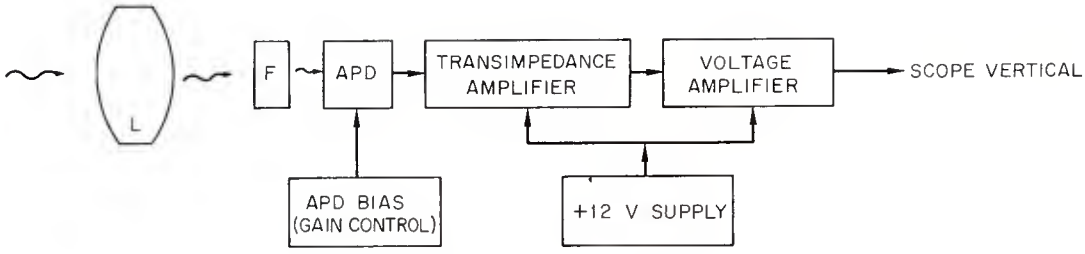

Figure 9. Receiver.

The design of the receiver circuitry presented few difficulties and called for little originality. However, the relative novelty of optical pulse ranging systems makes desirable a discussion in some detail.

The logical starting point in designing an optical receiver for a specific application is to choose a suitable photodiode and to design the signal amplifying and processing circuitry afterwards. However, one of the objects of this work was to evaluate photodiodes of various types of construction, and it was therefore the primary aim to reproduce the detected signals with sufficient fidelity for meaningful analysis. The requirements that emerged from these considerations were that (1) a 10-nA signal current should result in a 10-mV output signal, and (2) the video band-pass should exceed 10 MHz for photodiodes having junction capacitances up to 30 pF.

Within the band-pass required, photodiodes may be modelled by the equivalent circuit shown in figure 10. This is somewhat simplified: the noise and signal current generators have been lumped together without distinction, and the avalanche multiplication, if any, is assumed to have occurred. The capacitance and resistance of the depletion layer, R_d and C_d, are on the order of 10^7 ohms and 3 to 30 pF, respectively. Series resistance R_s represents the sum of the contact resistances and the resistance of the undepleted bulk semiconductor material. Depending on the diode construction, R_s may assume values from 5 to 500 ohms, although 20 to 100 ohms was more typical of the diodes with which we dealt.

Assume now that a load resistance, R_L, has been connected to the photodiode terminals and that a stimulus applied to the photodiode results in a unit step of current. Since $R_d >> (R_s + R_L)$, it may be ignored. Hence, the current developed in R_L rises as $\exp\left[-t/(R_s + R_L)C_d\right]$ with a rise time approximated by $t_r = 2.2\,(R_s + R_L)C_d$. Requiring a video bandwidth B > 10 MHz is approximately equivalent to requiring $t_r < 35$ ns. Assuming a worst-case C = 30 pF, $t_r < 35$ ns for $(R_s + R_L) < 530$ ohms. If R_s = 100 ohms, then

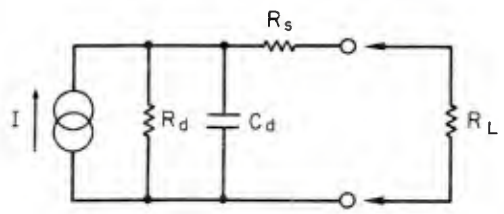

Figure 10. Photodiode equivalent circuit.

R_L < 430 ohms. A satisfactory means of presenting a low impedance to the photodiode and at the same time achieving useful gain is to use an operational amplifier connected as a transimpedance amplifier (fig. 11). Ideally, the resistance looking into the summing junction is R_f/A_v, where the open-loop voltage gain is $-A_v$. Even the very simple circuit used in this project (fig. 12) can achieve a sufficiently low input resistance that the detector capacitance does not limit the rise time. Instead, the upper cutoff frequency is determined by the combination of R_f with its own parasitic capacitance, C_f.

The complete receiver including the voltage amplifier is diagrammed in figure 13. It is fair to say that many of the components were included to protect against overload or accidental misconnection. Thus, network C1-D2-D3-R1-C2 clips large transients before they can reach IC1. Resistor R2 was made quite large to limit the photodiode current, in the event that the avalanche voltage might be much exceeded, such as by a power-supply switching transient. Operating from a single 12-V supply required a Zener regulator (D4) to establish

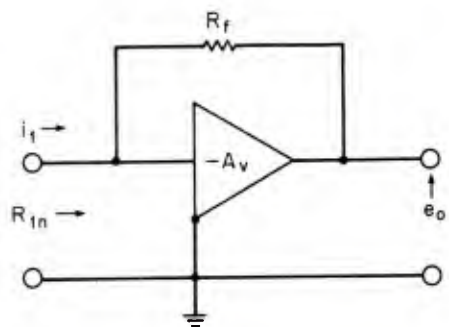

FOR A_v LARGE, $R_{in} \rightarrow 0$
AND $e_o \sim i_1 R_f$

Figure 11. Transimpedance concept.

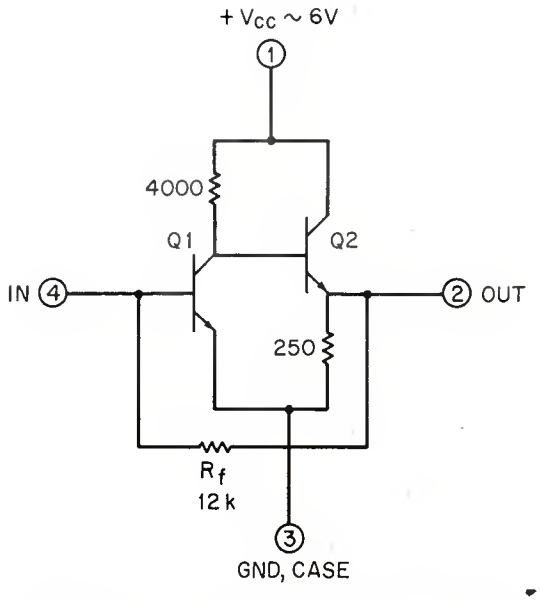

Figure 12. Circuit of TIXL152.

the correct bias for IC1 and at the same time imposed ac coupling between the stages. Resistors R4, R8, and R13 provide a dc return for the coupling capacitors C3, C10, and C11, thus protecting the IC's and transistor Q1 from large surge currents when changing connections with the power on.

The voltage amplifier consisted of a single Fairchild 733 wide-band video amplifier IC, connected for maximum gain. The output swing of this IC is severely limited when driving 50-ohm loads directly, and an emitter-follower was therefore added as a cable driver. Resistor R11 was selected empirically to make the output impedance 50 ohms, so that the scope connection might be left unterminated without incurring distortion from the reflection. The completed voltage amplifier had a voltage gain of 83 with the output terminated or 166 into a high-impedance load, the response rolling off gradually above 10 MHz (-3 dB at 40 MHz). This IC proved unsuitable for low-level amplification, chiefly because the several samples tried all displayed "popcorn" or "burst" noise. It was empirically observed that this noise could be reduced by connecting a small resistor across the input terminals. Thus, the cable terminating resistor was moved there (R9 in figure 13), and the input coupling capacitor was increased to maintain low-frequency response.

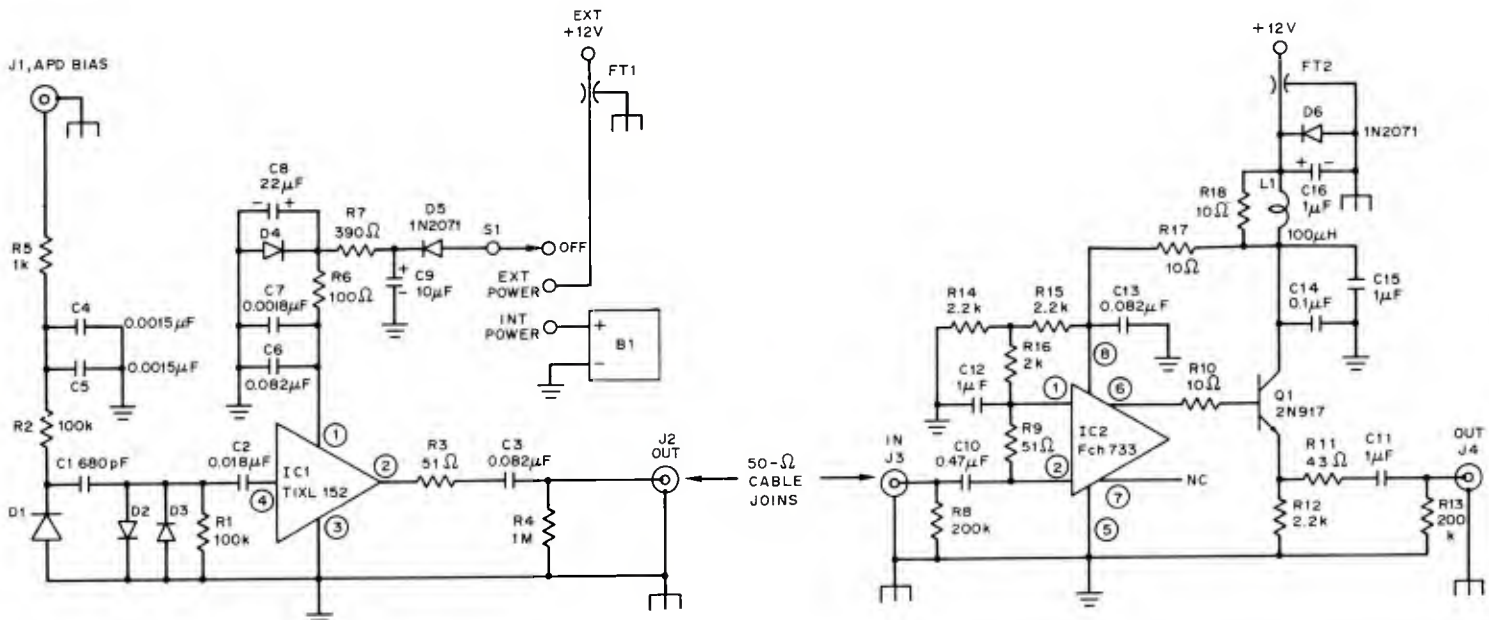

D1 AVALANCHE PHOTODIODE
D2 1N4154
D3 1N4154
D4 ZENER, 6.4V, 400 mW
D5 1N2071
D6 1N2071

NOTE: IC2, Fch 733, TO-100 PACKAGE PIN CONNECTION SHOWN. PINS 4-9 SHORTED TOGETHER FOR MAXIMUM GAIN.

Figure 13. Entire receiver circuit.

Lastly, the amplifier bias supplies are extensively decoupled. This was a consequence of the transmitter construction, which was unshielded for ease of access. For this reason, also, it proved useful in testing to have the alternative of powering the preamplifier from its own internal battery, rather than from the external 12-V source. In my experience, virtually total electrical isolation of the receiver from the transmitter can be obtained, even if the two are physically adjacent, but careful attention to shielding and decoupling is necessary to achieve this. The experimental results obtained with this receiver are given by Holland and Wellman.[2] However, the noise performance is limited in this instance by background radiation, rather than by amplifier noise.

---

[2] *R. Holland and R. Wellman, Feasibility Demonstration of a Slant-Range Optical Proximity Sensor (U), Harry Diamond Laboratories TM-74-17 (December 1974). (CONFIDENTIAL)*

APPENDIX A.--EMPIRICAL RELATIONSHIPS IN THE DISCHARGE CIRCUIT

This appendix comprises two graphs (fig. A-1, A-2). One relates the width of the discharge current pulse to the value of the storage capacitance, and the other depicts the voltage required on the storage capacitor prior to discharge, to achieve a given injection current, I_{pk}. These graphs are intended as a design aid and are not presented as closely predictive of circuit performance. These data apply only to circuits using either the SSPI type GA-201 silicon-controlled rectifier (SCR) or other SCR's having similar terminal characteristics. In the course of the experiment, the SCR's were sometimes operated above their normal rating of V_{fx} = 100 V. This is not recommended as a production measure. Furthermore, data were gathered for injection currents up to 50 A, which would appear to exceed the allowable injection current. The pulse widths, however, were considerably shorter than the 200-ns pulse width for which the maximum allowable forward current, I_{fm}, is specified, so that the average input power to the laser was held within a reasonable limit.

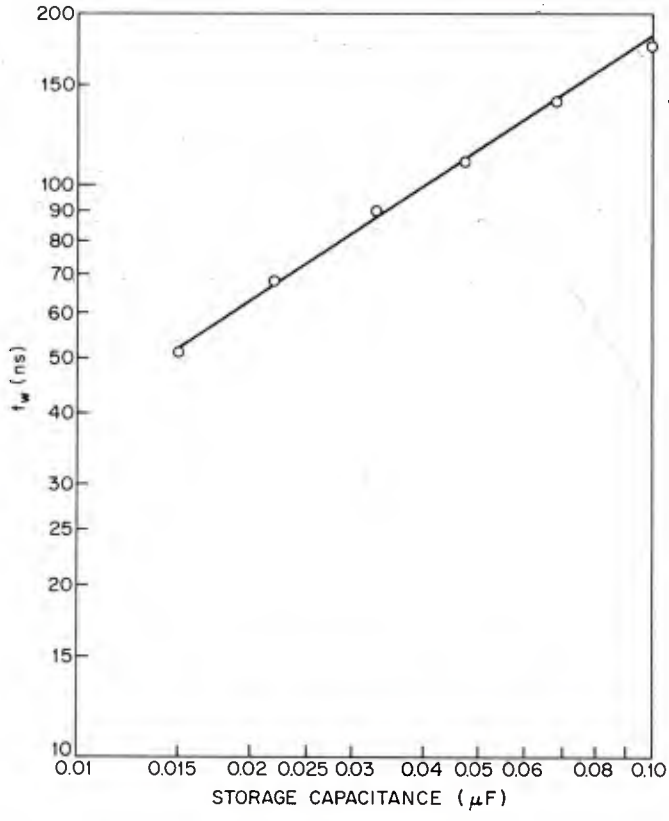

Figure A-1. Width of discharge pulse as function of storage capacitance.

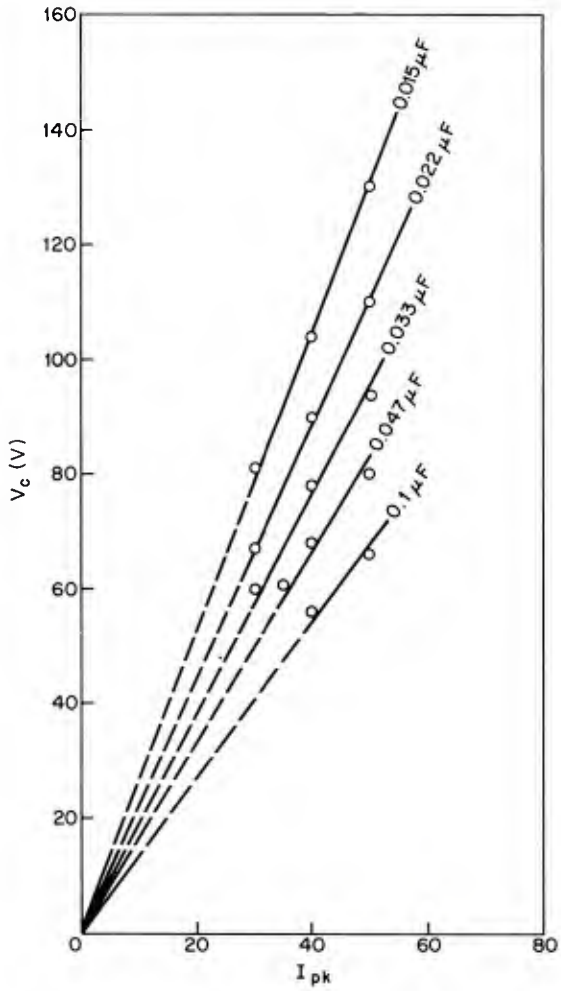

Figure A-2. V_c required to produce given I_{pk} for various values of storage capacitance (dashed line indicates projection through origin).

APPENDIX B.--ANALYSIS OF THE RESONANT CHARGING CIRCUIT

The resonant charging circuit, although theoretically lossless, is in practice subject to losses that can be considerable. In this appendix, the effect of the principal losses on the circuit operation is investigated at some length, and practical examples are given.

The discussion that follows is based on the series resonant circuit model shown in figure B-1. It is assumed that the diode drop may be subtracted from V_s and that all stray circuit resistances may be lumped together in the single resistor, R. At time t = 0, switch S is closed, and a current, i = i(t), begins to flow in the loop according to

$$Ri + L\frac{di}{dt} + \frac{1}{C}\int_0^t i\,dt = V_s \qquad \text{(B-1)}$$

with the initial conditions that

$$i = 0 \quad \text{for } t \leq 0 \qquad \text{(B-2)}$$

and

$$V_c = 0 \text{ for } t \leq 0\ . \qquad \text{(B-3)}$$

Differentiating equation (B-1),

$$\frac{d^2i}{dt^2} + \frac{R}{L}\frac{di}{dt} + \frac{i}{LC} = 0\ , \qquad \text{(B-4)}$$

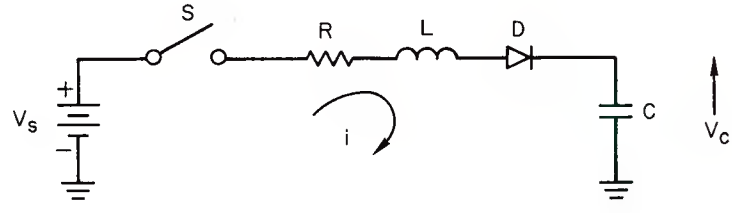

Figure B-1. Model of resonant charging circuit.

which has the general solution

$$i_g = Ae^{\lambda_+ t} + Be^{\lambda_- t} \quad , \tag{B-5}$$

in which

$$\lambda_\pm = \frac{1}{2} \left\{ \frac{-R}{L} \pm \left[\left(\frac{R}{L} \right)^2 - \frac{4}{LC} \right]^{\frac{1}{2}} \right\} \quad , \tag{B-6}$$

and A and B are undetermined constants.

Imposing the initial conditions of equation (B-2), equation (B-3) yields

$$A = -B \tag{B-7}$$

and

$$A = \frac{V_s}{L \left[\left(\frac{R}{L} \right)^2 - \frac{4}{LC} \right]^{\frac{1}{2}}} \quad . \tag{B-8}$$

Substituting equations (B-7) and (B-8) into equation (B-5) yields, after some manipulation, the particular solution

$$i(t) = \frac{2 V_s}{L \left[\frac{4}{LC} - \left(\frac{R}{L} \right)^2 \right]} \; e^{\frac{-Rt}{2L}} \sin \left\{ \frac{t}{2} \left[\frac{4}{LC} - \left(\frac{R}{L} \right)^2 \right]^{\frac{1}{2}} \right\} . \tag{B-9}$$

Restricting our interest to cases for which

$$\frac{4}{LC} > \left(\frac{R}{L} \right)^2 \quad , \tag{B-10}$$

the sign of i(t) changes for t greater than some t = T given by setting the argument in the sine term equal to π. Thus, at

$$T = \frac{2\pi}{\left[\frac{4}{LC} - \left(\frac{R}{L}\right)^2\right]^{\frac{1}{2}}}, \tag{B-11}$$

the current i reverses, turning off the diode, D, and ending the charging interval.

From equation (B-9), the voltage on the capacitor, $V_c(t)$ may be calculated for $0 \leq t \leq T$:

$$V_c(t) = \frac{1}{C}\int_0^t \frac{2\,V_s}{L\left[\frac{4}{LC} - \left(\frac{R}{L}\right)^2\right]^{\frac{1}{2}}} e^{\frac{-Rt}{2L}} \sin\left\{\frac{t}{2}\left[\frac{4}{LC} - \left(\frac{R}{L}\right)^2\right]^{\frac{1}{2}}\right\} dt \,. \tag{B-12}$$

By substitution of variables, this integral may be reduced to a tabulated form. Ultimately, one arrives at

$$V_c(t) = V_s\left[1 + e^{\frac{-Rt}{2L}}\left(\frac{-1}{\left[\frac{4}{LC} - \left(\frac{R}{L}\right)^2\right]^{\frac{1}{2}}} \sin\left\{\frac{t}{2}\left[\frac{4}{LC} - \left(\frac{R}{L}\right)^2\right]^{\frac{1}{2}}\right\} - \cos\left\{\frac{t}{2}\left[\frac{4}{LC} - \left(\frac{R}{L}\right)^2\right]^{\frac{1}{2}}\right\}\right)\right]. \tag{B-13}$$

At t = T, equation (B-13) reduces simply to

$$V_c(T) = V_s\left[1 + e^{\frac{-\pi}{\left(\frac{4L}{R^2C} - 1\right)^{\frac{1}{2}}}}\right] \,. \tag{B-14}$$

In equation (B-14), as $R \to 0$, $V_c \to 2\ V_s$. It is instructive to calculate $V_c(T)$ for real components. With R = 36 ohms, L = 4.7 mH, and C = 0.1 μF, $V_c = 1.77\ V_s$. Thus, the effect of series resistance is seen not to be negligible in calculating V_s. In the example given, the predominant source of R_s is the miniature ferrite choke. From equation (B-14), it is also plain that for a given L and R, decreasing C increases V_c. Continuing for example, if C = 0.02 μF, $V_c = 1.89\ V_s$. Thus, in the analytic prediction of V_c/V_s, it is advisable to include resistive loss. However, by substitution in equation (B-11), it may be demonstrated that the value of T is not appreciably affected by setting R = 0. Taking the above example with C = 0.1 μF and L = 4.7 mH,

$$T = 6.834 \times 10^{-5}\ s, \quad \text{for } R = 36 \text{ ohms},$$

and

$$T = 6.811 \times 10^{-5}\ s, \quad \text{for } R = 0 \text{ ohms},$$

an error of -0.35 percent.

This is negligible when compared with the tolerances on the values of L and C.

Thus, to design efficient circuits of this type, it is necessary to minimize resistance R. The chief source of this quantity in most practical circuits is inductor L, which must typically be made physically small, incurring the usual penalties of miniaturization. Furthermore, in choosing L, there exists an additional constraint: the maximum dV/dt developed across the SCR during the charging interval may not exceed the value $dV/dt|_{crit}$, or else the SCR is triggered by rate effect. The worst-case estimate of these quantities can be made by assuming R = 0, in which case equation (B-9) for i(t) becomes

$$i(t) = V_s \left(\frac{C}{L}\right)^{\frac{1}{2}} \sin \frac{t}{(LC)^{\frac{1}{2}}}, \tag{B-15}$$

whence

$$I_{max} = V_s \left(\frac{C}{L}\right)^{\frac{1}{2}} \tag{B-16}$$

and

$$\max \frac{dV_c}{dt} = \frac{I_{max}}{C} = \frac{V_s}{(LC)^{\frac{1}{2}}}. \tag{B-17}$$

Thus, to prevent rate-effect triggering of the SCR, set

$$\frac{V_s}{(LC)^{\frac{1}{2}}} < \left.\frac{dV}{dt}\right|_{crit} \quad . \tag{B-18}$$

Referring to the example, if L = 4.7 mH, C = 0.1 μF, and assuming that V_S = 50 V, substitution in equation (B-17) yields max dV_C/dt = 2.31 x 10^6 V/s, which is very much smaller than $dV/dt|_{crit}$ = 20 × 10^6 V/s.

DEFENSE DOCUMENTATION CENTER
CAMERON STATION, BUILDING 5
ALEXANDRIA, VA 22314
ATTN DDC-TCA (12 COPIES)

COMMANDER
USA RSCH & STD GP (EUR)
BOX 65
FPO NEW YORK 09510
ATTN LTC JAMES M. KENNEDY, JR.
CHIEF, PHYSICS & MATH BRANCH

COMMANDER
US ARMY MATERIEL DEVELOPMENT
& READINESS COMMAND
5001 EISENHOWER AVENUE
ALEXANDRIA, VA 22333
ATTN DRXAM-TL, HQ TECH LIBRARY
ATTN DRCDL, DEP FOR LABORATORIES
ATTN DRCRD, DIR RES, DEV & ENG
ATTN DRCRD-F, AIR SYSTEMS DIV
ATTN DRCRD-T, RESEARCH DIV
ATTN DRCRD-W, WEAPONS/MUNITIONS
SYSTEMS DIVISION

COMMANDER
USA ARMAMENT COMMAND
ROCK ISLAND, IL 61201
ATTN DRSAR-ASF, FUZE DIV
ATTN DRSAR-RDF, SYS DEV DIV - FUZES
ATTN DRSAR, GEORGE R. TAYLOR
ATTN TECHNICAL LIBRARY

COMMANDER
USA MISSILE & MUNITIONS CENTER
& SCHOOL
REDSTONE ARSENAL, AL 35809
ATTN ATSK-CTD-F

DIRECTOR
US ARMY BALLISTIC RESEARCH
LABORATORIES
ABERDEEN PROVING GROUND, MD 21005
ATTN DRXRD-BD, BALLISTIC RESEARCH LABS
ATTN DRXRD-BTL, FRANK J. ALLEN

COMMAND
US ARMY ELECTRONICS COMMAND
FORT MONMOUTH, NJ 07703
ATTN DRSEL-GG, TECHNICAL LIBRARY
ATTN DRSEL-TL-PT, B. LOUIS
ATTN DRSEL-TL-SM, DR. E. SCHIEL
ATTN DRSEL-CT, DR. R. G. BUSER
ATTN DRSEL-PP/P, MR. J. E. SANDERS

COMMANDER
US ARMY ELECTRONICS COMMAND
FORT BELVOIR, VA 22060
ATTN DRSEL-NV, LIBRARY
ATTN DRSEL-NV, S. B. GIBSON
ATTN DRSEL-NV, R. SHURTZ

COMMANDER
US ARMY MISSILE RESEARCH DEVELOPMENT
AND ENGINEERING LABORATORY
US ARMY MISSILE COMMAND
REDSTONE ARSENAL, AL 35809
ATTN DRSMI-RB, REDSTONE SCIENTIFIC
INFORMATION CENTER
ATTN DRSMI-RR, DR. J. P, HALLOWES

DIRECTOR
DEFENSE ADVANCED RESEARCH PROJECTS
AGENCY
ARCHITECT BUILDING
1400 WILSON BLVD
ARLINGTON, VA 22209
ATTN TECH INFO OFC

DIRECTOR OF DEFENSE RES AND
ENGINEERING
WASHINGTON, DC 20301
ATTN TECHNICAL LIBRARY (RM3C 128)

COMMANDER
EDGEWOOD ARSENAL
EDGEWOOD ARSENAL, MD 21010
ATTN SAREA-TS, TECHNICAL INFORMATION

COMMANDER
FRANKFORD ARSENAL
BRIDGE & TACONY STREETS
PHILADELPHIA, PA 19137
ATTN K1000, TECHNICAL LIBRARY
ATTN L5000, J. HELFRICH
ATTN W1000, AMRDC-AMC LASER SAFETY
TEAM

COMMANDER
PICATINNY ARSENAL
DOVER, NJ 07801
ATTN SARPA-TS, TECHNICAL LIBRARY

COMMANDER
US ARMY TANK-AUTOMOTIVE COMMAND
WARREN, MI 48089
ATTN DRSTA-RG, O. RENIUS

COMMANDER
HQ, US ARMY TEST & EVALUATION
COMMAND
ABERDEEN PROVING GROUND, MD 21005
ATTN DRSTE-AD-B, TECH INFO CENTER
ATTN DRSTE-SA-E, J. BIALO

COMMANDER
US ARMY ABERDEEN PROVING GROUND
ABERDEEN PROVING GROUND, MD 21005
ATTN STEAP-MTI, INFANTRY & AIRCRAFT WPNS

COMMANDER
US ARMY WEAPONS COMMAND, HQ
ROCK ISLAND, IL 61201
ATTN SWERR-PL, TECHNICAL LIBRARY
ATTN DRSWE-RER, E. VAUGHN

OFFICE, CHIEF OF RESEARCH,
DEVELOPMENT AND ACQUISITION
DEPARTMENT OF THE ARMY
WASHINGTON, DC 20310
ATTN DAMA-DD, DIR/DEVELOPMENTS
ATTN DAMA-ARP-P, DR. R. B. WATSON

COMMANDER
ARMY RESEARCH OFFICE (DURHAM)
RESEARCH TRIANGLE PARK, NC 27709
ATTN DR. ROBERT J. LONTZ

COMMANDER
ARMY MATERIALS & MECHANICS RESEARCH
CENTER
WATERTOWN, MA 02172
ATTN DRXMR-P, RAYMOND L. FARROW
ATTN DRXMR-ATL, TECH LIBRARY BR

COMMANDER
NATICK LABORATORIES
NATICK, MA 01762
ATTN DRXRES-RTL, TECHNICAL LIBRARY

COMMANDER
US ARMY MATERIEL SYSTEMS ANALYSIS AGENCY
ABERDEEN PROVING GROUND, MD 21005

COMMANDER
SPACE AND MISSILE SYSTEMS
ORGANIZATION
P.O. 96960
WORLDWAYS POSTAL CENTER
LOS ANGELES, CA 90009
ATTN RSSG, CAPT. EDMONDSON

COMMANDER
US ARMY ELECTRONICS COMMAND
OFC OF MSL ELECTRONICS WARFARE
WHITE SANDS MISSILE RANGE, NM 88002
ATTN DRSEL-BL, LIBRARY

COMMANDER
NAVAL AIR SYSTEMS COMMAND, HQ
DEPT OF THE NAVY
ARLINGTON, VA 20360
ATTN NAIR-604, TECH LIBRARY DIV

COMMANDER
NAVAL SURFACE WEAPONS CENTER
WHITE OAK, MD 20910
ATTN 1-315, TECH LIBRARY
ATTN CODE 423, D. KIRKPATRICK

COMMANDER
NAVAL SEA SYSTEMS COMMAND
DEPT OF THE NAVY
WASHINGTON, DC 20362
ATTN NSEA-0632, LIBRARY BRANCH

DIRECTOR
NAVAL RESEARCH LABORATORY
WASHINGTON, DC 20390
ATTN CODE 2620, TECHNICAL LIBRARY BR

COMMANDER
NAVAL WEAPONS CENTER
CHINA LAKE, CA 93555
ATTN CODE 353, ELECTRO-OPTICAL DIV
ATTN CODE 50, FUZE DEPARTMENT
ATTN CODE 753, LIBRARY DIVISION

COMMANDER
NAVAL SURFACE WEAPONS CTR
DAHLGREN, VA 22448
ATTN TECHNICAL LIBRARY, C. C. LYON
ATTN CODE FGE, DAVID TROYER

COMMANDER
AF AVIONICS LABORATORY, AFSC
WRIGHT-PATTERSON AFB, OH 45433
ATTN TEL, LASER & ELECTRO-OPTIC TECH BR
ATTN TEO, R. L. HARRIS

COMMANDER
AF WEAPONS LABORATORY, AFSC
KIRTLAND AFB, NM 87117
ATTN TECHNICAL LIBRARY

COMMANDER
ARMAMENT DEVELOPMENT AND TEST
CENTER
EGLIN AIR FORCE BASE, FL 32542
ATTN ADTC(DLOSL), TECH LIBRARY
ATTN DLJF, D. KEENE

HARRY DIAMOND LABORATORIES
ATTN MCGREGOR, THOMAS, COL, COMMANDING
OFFICER/FLYER, I.N./LANDIS, P.E./
SOMMER, H./CONRAD, E.E.
ATTN CARTER, W.W., DR., ACTING TECHNICAL
DIRECTOR/MARCUS, S.M.
ATTN KIMMEL, S., IO
ATTN CHIEF, 0021
ATTN CHIEF, 0022
ATTN CHIEF, LAB 100
ATTN CHIEF, LAB 200
ATTN CHIEF, LAB 300
ATTN CHIEF, LAB 400
ATTN CHIEF, LAB 500
ATTN CHIEF, LAB 600
ATTN CHIEF, DIV 700
ATTN CHIEF, DIV 800
ATTN CHIEF, LAB 900
ATTN CHIEF, LAB 1000
ATTN RECORD COPY, BR 041
ATTN HDL LIBRARY (3 COPIES)
ATTN CHAIRMAN, EDITORIAL COMMITTEE
ATTN CHIEF, 047
ATTN TECH REPORTS, 013
ATTN PATENT LAW BRANCH, 071
ATTN MCLAUGHLIN, P.W., 741
ATTN CHIEF, 910
ATTN CHIEF, 930
ATTN CHIEF, 940
ATTN WILLIAMS, D., 930
ATTN TUCKER, R., 930
ATTN HUMPHREY, R., 930
ATTN HATTERY, W., 930
ATTN VANDERWALL, J., 930 (10 COPIES)
ATTN MCGUIRE, D., 930
ATTN WILLIAMS, R., 930
ATTN BLACKBURN, J., 330